PERSISTENCE OF THE LAMINAR REGIME IN A FLAT PLATE BOUNDARY LAYER AT VERY HIGH REYNOLDS NUMBER

by

Jovan JOVANOVIĆ, Bettina FROHNAPFEL, Edin ŠKALJIĆ, and Milenko JOVANOVIĆ

Original scientific paper
UDC: 532.517.2/.4:533.6.011
BIBLID: 0354-9836, *10* (2006), 2, 63-96

Starting from the Navier-Stokes and the continuity equations of a viscous incompressible fluid, a statistical theory is developed for the prediction of transition and breakdown to turbulence in a laminar boundary layer exposed to small, statistically stationary axisymmetric disturbances. The transport equations for the statistical properties of the disturbances are closed using the two-point correlation technique and invariant theory. By considering the local equilibrium to exist between production and viscous dissipation, which forces the energy of the disturbances in the boundary layer to be lower than that of the free stream, the transition criterion is formulated in terms of the anisotropy of the disturbances and a Reynolds number based on the intensity and the length scale of the disturbances. The transition criterion determines conditions that guarantee maintenance of the laminar flow regime in a flat plate boundary layer. It is shown that predictions of the transition onset deduced from the transition criterion yield the critical Reynolds number, which is in good agreement with the experimental data obtained under well-controlled laboratory conditions reported in the literature. For the preferred mode of the axisymmetric disturbances, for which the intensity of the disturbances in the streamwise direction is larger than in the other two directions, the analysis shows that the anisotropy increases the critical Reynolds number. Theoretical considerations yield the quantitative estimate for the minimum level of the anisotropy of the free stream required to prevent transition and breakdown to turbulence. The numerical databases for fully developed turbulent wall-bounded flows at low and moderate Reynolds numbers were utilized to demonstrate the stabilizing and destabilizing role of the anisotropy in the disturbances on the development of the transition process in wall-bounded flows. The stabilizing role of increased anisotropy in a free stream on the boundary layer development was successfully tested experimentally in a large wind tunnel by maintaining the stable laminar regime in a flat plate boundary layer up to $(Re_x)_T \quad 4 \cdot 10^6$.

Key word: *transition, flow control, boundary layer theory, turbulence*

Introduction

The question of whether the laminar flow regime in a flat plate boundary layer can persist at high Reynolds numbers is of fundamental and practical importance. Taylor

[1] concluded, from the analysis of the boundary layer equations, that in absence of any external disturbances the laminar regime can persist up to infinite Reynolds number. The experimental work carried out by Dryden [2] showed that the point of transition from laminar to turbulent flow depends on the level of turbulence of the free stream. For small intensities of turbulence he found that the boundary layer remained laminar up to $(\mathrm{Re}_x)_T = x_1 U_\infty / \nu \quad 1.1 \cdot 10^6$, where x_1 is the distance from the leading edge of the plate, U_∞ is the velocity of the free stream and ν is the kinematic viscosity of the fluid. Later investigations by Schubauer and Skramstad [3] conducted in the Dryden wind tunnel (which is still in use at the University of Southern California) with a very low level of the background turbulence revealed that the transitional Reynolds number can be increased up to $(\mathrm{Re}_x)_T \quad 2.8 \cdot 10^6$. They found that the transition point moved progressively towards higher Reynolds numbers with decreasing the free stream turbulence until the relative value of 0.08% was attained. Further reduction of free stream turbulence did not result in an increase of $(\mathrm{Re}_x)_T$. In the subsequent experiments, Wells [4] and Spangler and Wells [5] obtained the transition Reynolds number $(\mathrm{Re}_x)_T \quad 5.25 \cdot 10^6$, which was nearly double that of Schubauer and Skramstad. They argued that not only the level of turbulence but also the energy spectrum and the nature of the disturbances has to be taken into consideration. Exceptionally large values of the transition Reynolds number were also reported by Saric and Reynolds [6], who obtained $(\mathrm{Re}_x)_T \quad 3.4 \cdot 10^6$ in a former NASA-Langley stability tunnel (currently under operation at the Virginia Polytechnic Institute, Blacksburg), Kachanov, Kozlov and Levchenko [7] $(\mathrm{Re}_x)_T \quad 4.3 \cdot 10^6$ in the ITAM--Novosibirsk tunnel specially designed for investigations of the laminar turbulent transition process and by S. Bake (1999, personal communication) $(\mathrm{Re}_x)_T \quad 3.6 \cdot 10^6$ in the laminar wind tunnel of the Herman-Föttinger Institute of the Technical University Berlin.

The most careful work to date was carried out by Pfenninger [8]. In a series of experiments, he managed to reduce the disturbances in the entry region of the pipe flow to an extremely low level and reach the highest value of the transition Reynolds number of $(\mathrm{Re}_x)_T \quad 50 \cdot 10^6$, which is close to the corresponding values of the wing sections of commercial aircraft. In interpretation of the above result one must, however, account for the stabilizing effect of the flow acceleration in the entry region of the pipe. Hinze [9] estimated that owing to this stabilizing effect the above value of $(\mathrm{Re}_x)_T$ should be decreased by at least a factor of ten in order to be comparable to the data obtained in flat plate boundary layers.

All of the evidence mentioned above suggests that the laminar regime in a boundary layer can be maintained at very high Reynolds numbers. Although there has been an explosion of activity during the last two decades, exploring theoretical, experimental, and numerical capabilities, the overall progress achieved in understanding the interaction mechanisms between the free stream disturbances and the boundary layer is disappointingly slow. The systematic quantitative prediction of transition is a painful issue and techniques capable of controling transition *rationally* are lacking. An attempt is made here to shed new light on this basic problem of the boundary layer receptivity by considering the influence of the anisotropy in the free stream disturbances on the evolution of the laminar-turbulent transition process and at the same time provide useful hints about how to alter the anisotropy in the free stream disturbances in order to achieve

effective control over the transition process in a boundary layer and in this way achieve significant drag reduction at high Reynolds numbers.

The theory of transition and breakdown to turbulence in the boundary layer can be worked out for small statistically stationary disturbances proceeding from the basic equations that govern the "apparent" stresses and by using (*but not misusing*) the closure based on the application of the two-point correlation technique and invariant theory [19]. Conclusions emerging from the theory can be tested by direct comparisons with numerical simulations or experiments. The mechanism responsible for transition can be identified without appeal to the empirical input or *ad hoc* approximation. However, its description might not be digestible for those who reason about transition in a deterministic fashion and exclusively in the physical space where observations usually take place: exposition and use of arguments and resulting deductions may therefore seem at first glance superficial, shallow, unreasonable, confusing or entirely wrong. If the matter is analyzed (with an open mind) in the functional space formed by the two scalar invariants which emphasize the anisotropy in the disturbances, the problem of transition and breakdown to turbulence under most common circumstances turns out to be the first one to attack because of its simplicity. Specific and unconventional use of arguments then appear logical and transparent. By arguing in the real space and the functional space it was possible to extract the criterion for transition onset in terms of the statistical properties of the free stream disturbances. This was the way which led us to a profound understanding and parametrization of the chief mechanism involved in polymer drag reduction [10] and we will follow a similar path in attacking the problem of the laminar to turbulent transition.

In a recent study, Jovanovi} and Pashtrapanska [11] used statistical techniques for the treatment of the transition process and derived an approximate set of closed equations for the behavior of the statistical properties of small, two-component, three-dimensional disturbances in a laminar boundary layer. By considering the local equilibrium to exist between production and viscous dissipation, which forces the level of the disturbances in the boundary layer to be lower than that of the free stream, the transition criterion was formulated in terms of a Taylor Reynolds number:

$$(\mathrm{Re}_{\lambda})_{\mathrm{crit}} \quad 10\sqrt{5} \tag{1}$$

based on the intensity q and the Taylor length-scale λ of the disturbances $\mathrm{Re}_{\lambda} = q\lambda/\nu$. The transition criterion emerges from the qualitative analysis of the dissipation rate equation, which was restricted to be valid only in a certain range of Taylor Reynolds numbers in order to prevent any possibility that the dissipation rate in the boundary layer assumes negative values, which is physically impossible. The experimental and numerical databases for fully developed turbulent flows at low Reynolds numbers were utilized to demonstrate the validity of the derived transition criterion for the estimation of transition onset and breakdown to turbulence in wall-bounded flows. By extrapolating the trends in these databases towards the derived transition criterion, the critical Reynolds numbers for channel, pipe, and boundary layer flows were obtained in close agreement with accumulated observations available from either numerical simulations or experiments.

The two-component considerations can be extended to more realistic situations involving statistically axisymmetric disturbances. Axisymmetry is the most common state of the disturbances in nature, since such disturbances can satisfy constraints dictated by the continuity equation close to the wall and also the boundary conditions in the free stream. The statistical analysis of the dynamic equations for axisymmetric disturbances permits the identification of the role which the anisotropy in the free stream disturbances plays during the transition process. We intend to approach the outstanding question of transition in a laminar boundary layer by studying the influence of the anisotropy on the dynamics of small axisymmetric disturbances in a laminar boundary layer and in this way learn something more fundamental about transition and breakdown to turbulence that has been overlooked in previous studies of the subject.

The aim of this paper is to contribute further to the theoretical and more importantly to the *practical* understanding of the transition process using statistical techniques. An effort is made to provide a quantitative description of laminar to turbulent transition using stochastic tools suitable for describing random, three-dimensional flow fields. We shall provide rational approximations for the mechanisms involved during the transition process using the two-point correlation technique and invariant theory and finish with a closed set of approximate equations from which it is possible to formulate the criterion for the determination of transition onset in a flat plate boundary layer. An account is given of an analytical investigation which demonstrates the stabilizing and destabilizing role of the anisotropy in the disturbances on the transition process. An experimental investigation carried out in the large wind tunnel of the Lehrstuhl für Strömungsmechanik (LSTM) in Erlangen in which the anisotropy in the free stream disturbances was sufficiently high confirmed all essential features of the transition process predicted by the developed theory. This provided support for the results emerging from the theory in respect of flow control and maintenance of a stable laminar regime in a flat plate boundary layer at very high Reynolds numbers.

Basic equations for small disturbances

Starting from the Navier-Stokes and the continuity equations of a viscous incompressible fluid:

$$\frac{\partial u_i}{\partial t} \quad u_k \frac{\partial u_i}{\partial x_k} \qquad \frac{1}{\rho}\frac{\partial p}{\partial x_i} \quad \nu \frac{\partial^2 u_i}{\partial x_k \partial x_k}, \quad i,k \quad 1,2,3 \tag{2}$$

$$\frac{\partial u_k}{\partial x_k} \quad 0 \tag{3}$$

and introducing the conventional method of separating the instantaneous velocity u_i and the pressure p into the mean laminar flow and a disturbance u_i and p superimposed on it:

$$u_i \quad U_i \quad u_i, \quad p \quad P \quad p \tag{4}$$

one obtains the equations for the disturbances:

$$\frac{\partial u_i}{\partial t} \quad U_k \frac{\partial u_i}{\partial x_k} \quad u_k \frac{\partial U_i}{\partial x_k} \qquad \frac{1}{\rho}\frac{\partial p}{\partial x_i} \quad \nu \frac{\partial^2 u_i}{\partial x_k \partial x_k} \tag{5}$$

$$\frac{\partial u_k}{\partial x_k} \quad 0 \tag{6}$$

In the derivation of the above equations, it is assumed that the disturbances are much smaller than the corresponding quantities of the mean laminar flow:

$$u_i \ll U_i, \quad p \ll P \tag{7}$$

and that it satisfies the Navier-Stokes and the continuity equations:

$$U_k \frac{\partial U_i}{\partial x_k} \qquad \frac{1}{\rho}\frac{\partial P}{\partial x_i} \quad \nu \frac{\partial^2 U_i}{\partial x_k \partial x_k} \tag{8}$$

$$\frac{\partial U_k}{\partial x_k} \quad 0 \tag{9}$$

By systematic manipulation of eqs. (5) and (6), it is possible to obtain equations for the "apparent" stresses – see, for example, [9 (pp. 323-324)]:

$$\frac{\partial \overline{u_i u_j}}{\partial t} \quad U_k \frac{\partial \overline{u_i u_j}}{\partial x_k}$$

$$\overline{u_j u_k}\frac{\partial U_i}{\partial x_k} \quad \overline{u_i u_k}\frac{\partial U_j}{\partial x_k} \underbrace{\frac{1}{\rho}\overline{u_j \frac{\partial p}{\partial x_i}} \quad \overline{u_i \frac{\partial p}{\partial x_j}}}_{\Pi_{ij}} \underbrace{2\nu \overline{\frac{\partial u_i}{\partial x_k}}\overline{\frac{\partial u_j}{\partial x_k}}}_{\varepsilon_{ij}} \quad \nu \frac{\partial^2 \overline{u_i u_j}}{\partial x_k \partial x_k} \tag{10}$$

In the above equations, one can identify two different types of unknown correlations: the velocity-pressure gradient correlations Π_{ij} and the dissipation correlations ε_{ij} These correlations must be expressed in terms of known quantities U_i and $\overline{u_i u_j}$ in order to close the resultant eq. (10) for the "apparent" stresses.

The closure problem for small axisymmetric disturbances

Let small disturbances be statistically axisymmetric so that all correlations involved in eq. (10) are invariant under rotation about the common axis defined by the arguments of the unit vector $\vec{\lambda}$ [12]:

$$\begin{array}{lcll} \overline{u_i u_j} & = & A\delta_{ij} & B\lambda_i\lambda_j \\ \varepsilon_{ij} & & C\delta_{ij} & D\lambda_i\lambda_j \\ \Pi_{ij} & & E\delta_{ij} & F\lambda_i\lambda_j \end{array} \tag{11}$$

where *A*-*F* are scalar functions that need to be constructed from analytical considerations. For such disturbances, it is possible to attack the closure of eq. (10) using the two-point correlation technique developed by Chou [13] and the invariant theory introduced by Lumley and Newman [14].

Application of the two-point correlation technique permits the separation of the inhomogeneous effects in treatment of the unknown terms involved in eq. (10) and re-casting of the inhomogeneous problem into the corresponding one of a statistically homogeneous flow field.Then, using invariant theory, it is possible to isolate the effects of anisotropy in the "apparent" stresses from all other flow properties, which allows rational construction of the closure approximations that include all physically realistic states of axisymmetric disturbances.

Application of the two-point correlation technique for interpretation of ε_{ij}

Let us first consider closure for the terms which are related to the dissipation process:

$$\varepsilon_{ij} \quad \nu\overline{\frac{\partial u_i}{\partial x_k}\frac{\partial u_j}{\partial x_k}} \tag{12}$$

that appear in eq. (10). The most efficient procedure to treat these correlations is based on the two-point correlation technique that was originally developed by Chou [13] and subsequently refined by Kolovandin and Vatutin [15] and Jovanovi}, Ye and Durst [16]. However, application of this technique to the study of the dynamics of the disturbances is complicated, tedious and very demanding for the reader. Here we shall provide only a brief account of the parts of the subject which are relevant for the present study.

In order to separate the effect of local character from global, large-scale fluid motion, we must first express the dissipation correlations ε_{ij} in a coordinate system relative to two closely separated points A and B in space as follows:

$$\varepsilon_{ij} \quad \nu\overline{\frac{\partial u_i}{\partial x_k}\frac{\partial u_j}{\partial x_k}} \quad \nu \lim_{\substack{A\\B}} \overline{\frac{\partial u_i}{\partial x_k}_{A}\frac{\partial u_j}{\partial x_k}_{B}} \quad \nu \lim_{\substack{A\\B}} \frac{\partial}{\partial x_k}_{A}\frac{\partial}{\partial x_k}_{B}\overline{(u_i)_A (u_j)_B} \tag{13}$$

Expressing the partial differential operators in correlation (13) at points A and B as functions of the position in space and the relative coordinates between these two points:

$$\xi_k = (x_k)_B - (x_k)_A \tag{14}$$

and taking the limit A B yields [16]:

$$\varepsilon_{ij} \quad \nu\overline{\frac{\partial u_i}{\partial x_k}\frac{\partial u_j}{\partial x_k}} \quad \underbrace{\frac{1}{4}\nu\Delta_x\overline{u_i u_j}}_{\text{inhomogeneous}} \underbrace{\nu(\Delta_\xi\overline{u_i u_j})_0}_{\text{homogeneous}} \tag{15}$$

where the double prime (") indicates a value of the two-point correlation function at point B, $\overline{(u_i)_A (u_j)_B}$ $\overline{u_i u_j}$, the subscript $(_0)$ represents zero relative separation in space, $\vec{\xi}$ 0, and corresponds to the Laplace operator (Δ_x $^2/\ x_k\ x_k$ ξ $^2/\ \xi_k\ \xi_k$).

Equation (15) shows that ε_{ij} is composed of an inhomogeneous part $1/4\nu\Delta_x\overline{u_i u_j}$ and a homogeneous part ε_{ij}^h $\nu(\Delta_\xi\overline{u_i u_j})_0$. Since the tensor ε_{ij} is symmetrical, from (15) it follows that:

$$(\Delta_\xi\overline{u_i u_j})_0 \quad (\Delta_\xi\overline{u_j u_i})_0 \tag{16}$$

the two-point velocity correlation of second rank in the limit when $\vec{\xi}$ 0 satisfies the same relationship as in a statistically homogeneous flow field. This peculiarity of the two-point velocity correlation, deduced only from kinematic considerations, permits us to introduce the concept of local homogeneity for the disturbances, which leads to radical simplifications of the dynamic equations for the dissipation correlations.

Since the inhomogeneous part of ε_{ij} can be directly related to $\overline{u_i u_j}$ we need to consider only the homogeneous part of (15). Using the two-point correlation technique, kinematic constraints, and the continuity equation, it can be shown [13, 15, 17] that the components of the homogeneous part of (15) can be interpreted analytically in terms of its trace ε_h $\nu(\Delta_\xi\overline{u_s u_s})_0$ and the "apparent" stresses $\overline{u_i u_j}$ and that ε_h is related to the Taylor microscale λ as follows:

$$\varepsilon_h \quad 5\nu\frac{q^2}{\lambda^2} \tag{17}$$

Therefore, only the equation for ε_h needs to be considered. This equation is obtained by operating the dynamic equation for the two-point velocity correlation in a relative coordinate system with respect to $-\nu\Delta_\xi$ and setting $\vec{\xi}$ 0 to obtain [16]:

$$\begin{aligned} &\nu\frac{\partial}{\partial t}(\Delta_\xi\overline{u_s u_s})_0 \quad \nu U_k\frac{\partial}{\partial x_k}(\Delta_\xi\overline{u_s u_s})_0 \quad 2\nu(\Delta_\xi\overline{u_k u_s})_0\frac{\partial U_s}{\partial x_k} \\ &2\nu\ \frac{\partial^2}{\partial\xi_l\,\partial\xi_k}\overline{u_s u_s}\ _0\ \frac{\partial U_k}{\partial x_l} \quad 2\nu^2(\Delta_\xi\Delta_\xi\overline{u_s u_s})_0 \quad \frac{1}{2}\nu^2\Delta_x(\Delta_\xi\overline{u_s u_s})_0 \end{aligned} \tag{18}$$

The approximate equation for the homogeneous part of the dissipation rate involves only the derivatives of two-point velocity correlations. In the derivation of this equation, the concept of local homogeneity was utilized by applying the relationships for the derivatives of the two-point correlation functions for zero separation ($\vec{\xi}$ = 0) that are valid in a statistically homogeneous flow field.

The first two terms on the right-hand side of the approximate eq. (18) are the production terms that originate from the mean velocity gradient. The firm analytical closure for these terms can be formulated only for the case of axisymmetric disturbances. For such disturbances, Jovanovi}, Oti}, and Bradshaw [18] showed that the above-mentioned terms are equal, and their sum is given by:

$$2\nu(\Delta_\xi \overline{u_k u_s})_0 \frac{\partial U_s}{\partial x_k} \quad 2\nu \quad \frac{\partial^2}{\partial \xi_l \partial \xi_k} \overline{u_s u_s} \quad _0 \frac{\partial U_k}{\partial x_l} \qquad 2\mathcal{A} \frac{\varepsilon_h \overline{u_i u_k}}{k} \frac{\partial U_i}{\partial x_k} \tag{19}$$

where k $(1/2)\overline{u_k u_k}$ $1/2)q^2$ and $\mathcal{A}$ is the scalar function which depends on the anisotropy in $\overline{u_i u_j}$ and ε_{ij}^h, as specified in fig. 1, and will be discussed latter.

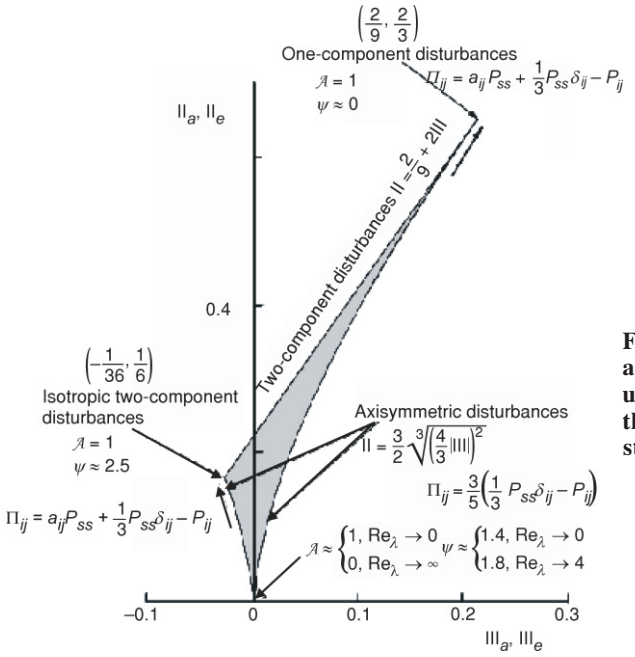

Figure 1. Anisotropy invariant map and the asymptotic forms for the unknown correlations involved in the equations for the "apparent" stresses

The third term on the right-hand side of eq. (18) represents the viscous destruction of ε_h and can be approximated using the result which holds in grid-generated turbulence:

$$2\nu^2(\Delta_\xi \Delta_\xi \overline{u_s u_s})_0 \qquad \psi \frac{\varepsilon_h^2}{k} \tag{20}$$

and by introducing modifications which take into account the influence of the anisotropy in the disturbances on ψ as shown in fig. 1 [18, 19 (pp. 51-64)].

Construction of the closure approximations using invariant theory

We shall now apply the invariant theory developed by Lumley and Newman [14] to formulate the closures for partition of the homogeneous part of the dissipation tensor and also for the velocity-pressure gradient correlations. These authors introduced the tensor:

$$a_{ij} \quad \frac{\overline{u_i u_j}}{q^2} \quad \frac{1}{3}\delta_{ij} \tag{21}$$

and its scalar invariants:

$$\mathrm{II}_a = a_{ij}a_{ji}, \qquad \mathrm{III}_a = a_{ij}a_{jk}a_{ki} \tag{22}$$

to quantify the anisotropy and define the limiting states of the disturbances. A cross plot of II_a *vs.* III_a for axisymmetric disturbances:

$$\mathrm{II}_a \quad \frac{3}{2}\sqrt[3]{\frac{4}{3}\left|\mathrm{III}_a\right|^2} \tag{23}$$

and two-component disturbances:

$$\mathrm{II}_a \quad \frac{2}{9} \quad 2\mathrm{III}_a \tag{24}$$

defines the anisotropy invariant map which, according to Lumley [20], bounds all physically realizable disturbances. This plot is shown in fig. 1 along with the asymptotic forms for scalar functions involved in the closure proposals for the unknown correlations in eq. (10) that can be derived for axisymmetric disturbances.

For axisymmetric disturbances, Jovanovi} and Oti} [21] showed that all second-rank correlation tensors involved in eq. (10) are linearly aligned in terms of each other. For such disturbances we may write:

$$e_{ij} \quad \mathcal{A}a_{ij}, \quad \mathcal{A} \quad \frac{\mathrm{II}_e}{\mathrm{II}_a} \tag{25}$$

where e_{ij} is the anisotropy tensor of the homogeneous part of ε_{ij}:

$$e_{ij} \quad \frac{\varepsilon_{ij}^h}{\varepsilon_h} \quad \frac{1}{3}\delta_{ij} \tag{26}$$

and

$$\mathrm{II}_e = e_{ij}e_{ji}, \qquad \mathrm{III}_e = e_{ij}e_{jk}e_{ki} \tag{27}$$

For limiting states of the axisymmetric disturbances, *i. e.* the two-component isotropic state and the one-component state it holds:

$$\mathrm{II}_a = \mathrm{II}_e \tag{28}$$

and therefore for these cases $\mathcal{A}$ is given by:

$$\mathcal{A}_{2C\text{–iso}} = 1 \tag{29}$$

$$\mathcal{A}_{1C} = 1 \tag{30}$$

For very small Reynolds numbers, when $\mathrm{Re}_\lambda \to 0$, the dissipation and energy-containing ranges of the spectrum overlap, with little separation between the corresponding length scales, and therefore we may assume that [22]:

$$\mathcal{A} \to 1, \quad \mathrm{Re}_\lambda \to 0 \tag{31}$$

holds for arbitrary anisotropy in the disturbances.

For vanishing anisotropy in the disturbances and large Reynolds numbers, when $\mathrm{II}_a \to 0$ and $\mathrm{Re}_\lambda \to \infty$, we may explore the hypothesis of local isotropy in the sense suggested by Kolmogorov [23] and assume that:

$$\mathcal{A} \to 0, \quad \mathrm{II}_a \to 0, \quad \text{and} \quad \mathrm{Re}_\lambda \to \infty \tag{32}$$

For vanishing anisotropy in the disturbances and large Re_λ, the homogeneous part of the dissipation rate ε_h may be related to the "integral" length scale L_f of the energy-containing range [23, 24] by:

$$\varepsilon_h \to 0.192\frac{q^3}{L_f}, \quad \mathrm{Re}_\lambda \gg 1 \tag{33}$$

At very low Reynolds numbers, the relationship between λ and L_f can be derived analytically to yield ([9] p. 210):

$$L_f \to \frac{1}{2}\sqrt{\frac{\pi}{2}}\lambda, \quad \mathrm{Re}_\lambda \ll 1 \tag{34}$$

Using the above expression and expression (17), ε_h can be written as:

$$\varepsilon_h \to 1.959\nu\frac{q^2}{L_f^2}, \quad \mathrm{Re}_\lambda \ll 1 \tag{35}$$

Following the suggestion of Rotta [22], we combine the above asymptotic forms for ε_h to obtain the interpolation equation valid for low and high Reynolds numbers:

$$\varepsilon_h \to 1.959\nu\frac{q^2}{L_f^2} + 0.192\frac{q^3}{L_f} \tag{36}$$

With expresions (17) and (36) we can express the length scale ratio λ/L_f in terms of the Reynolds number:

$$\frac{\lambda}{L_f} \quad 0.0489\,\mathrm{Re}_\lambda \quad \frac{1}{2}\sqrt{0.00956\,\mathrm{Re}_\lambda^2 \quad 10.186} \tag{37}$$

which attains a maximum value of 1.595 when $\mathrm{Re}_\lambda \quad 0$ and vanishes for $\mathrm{Re}_\lambda \quad \infty$. It is suitable to normalize the above relation and introduce the function:

$$\mathcal{W} \quad \frac{1}{1.595}\frac{\lambda}{L_f} \quad 0.626\frac{\lambda}{L_f} \tag{38}$$

which can be used to match the limiting properties of invariant functions $\mathcal{A}$ and ψ in the limit $\mathrm{II}_a \quad 0$ for very low and very high Reynolds numbers specified in fig. 1:

$$\begin{array}{lllll} \mathcal{A} & \mathcal{W}\mathcal{A}_{\mathrm{Re}_\lambda \quad 0} & (1 \quad \mathcal{W})\mathcal{A}_{\mathrm{Re}_\lambda \quad \infty} & \mathrm{II}_a & 0 \\ \psi & \mathcal{W}\psi_{\mathrm{Re}_\lambda \quad 0} & (1 \quad \mathcal{W})\psi_{\mathrm{Re}_\lambda \quad \infty} & & \end{array} \tag{39}$$

Using (39), we find:

$$\begin{array}{llll} \mathcal{A} & \mathcal{W} & & \\ \psi & 1.8 \quad 0.4\mathcal{W} & \mathrm{II}_a & 0 \end{array} \tag{40}$$

The values of $\mathcal{A}$ and ψ at the limiting states of the disturbances shown in fig. 1 can be matched to (40) utilizing properties of the parameter J introduced by Lumley [20]:

$$J \quad 1 \quad 9 \quad \frac{1}{2}\mathrm{II}_a \quad \mathrm{III}_a \tag{41}$$

where $J = 0$ indicates the two-component disturbances and $J = 1$ corresponds to the state of vanishing anisotropy in the disturbances. Thus we may write approximate expressions for $\mathcal{A}$ and ψ for axisymmetric disturbances as:

$$\mathcal{A} \quad \begin{array}{llll} (1 \quad J)\mathcal{A}_{1\mathrm{C}} & J\mathcal{A}_{\mathrm{iso}} & \mathrm{III}_a & 0 \\ (1 \quad J)\mathcal{A}_{2\mathrm{C}\ \mathrm{iso}} & J\mathcal{A}_{\mathrm{iso}} & \mathrm{III}_a & 0 \end{array} \tag{42}$$

$$\psi \quad \begin{array}{llll} (1 \quad J)\psi_{1\mathrm{C}} & J\psi_{\mathrm{iso}} & \mathrm{III}_a & 0 \\ (1 \quad J)\psi_{2\mathrm{C}\ \mathrm{iso}} & J\psi_{\mathrm{iso}} & \mathrm{III}_a & 0 \end{array} \tag{43}$$

Taking relation (23), into account we obtain:

$$\mathcal{A} \quad \begin{array}{llll} 1 \quad 1 \quad 9\frac{1}{2}\mathrm{II}_a \quad \frac{3}{4}\sqrt{\frac{2}{3}\mathrm{II}_a}^{\,3} & (\mathcal{W} \quad 1) & \mathrm{III}_a & 0 \\ 1 \quad 1 \quad 9\frac{1}{2}\mathrm{II}_a \quad \frac{3}{4}\sqrt{\frac{2}{3}\mathrm{II}_a}^{\,3} & (\mathcal{W} \quad 1) & \mathrm{III}_a & 0 \end{array} \tag{44}$$

$$\psi \quad \begin{array}{ll} 1 \quad 9\frac{1}{2}\mathrm{II}_a \quad \frac{3}{4}\sqrt{\frac{2}{3}\mathrm{II}_a}^{\,3} & (1.8 \quad 0.4W) \quad \mathrm{III}_a \quad 0 \\ 22.5\frac{1}{2}\mathrm{II}_a \quad \frac{3}{4}\sqrt{\frac{2}{3}\mathrm{II}_a}^{\,3} & 1 \quad 9\frac{1}{2}\mathrm{II}_a \quad \frac{3}{4}\sqrt{\frac{2}{3}\mathrm{II}_a}^{\,3} \quad (1.8 \quad 0.4W) \quad \mathrm{III}_a \quad 0 \end{array} \tag{45}$$

On the basis of above analytic considerations, we may suggest an expression for partition of the dissipation tensor ε_{ij} for axisymmetric disturbances as follows:

$$\varepsilon_{ij} \quad \frac{1}{4}\nu\Delta_x\overline{u_i u_j} \quad \varepsilon_h \quad \frac{1}{3}(1 \quad \mathcal{A})\delta_{ij} \quad \mathcal{A}\frac{\overline{u_i u_j}}{q^2} \tag{46}$$

It can be shown that a Taylor series expansion near the wall for instantaneous disturbances leads to relations for the asymptotic behavior of the components of ε_{ij} in close agreement those with obtained from expression (46) [19 (p. 71)].

We may follow the same analytical path as outlined above for the treatment of the velocity pressure gradient correlations, which can be split into the pressure-transport term and the pressure-strain term:

$$\Pi_{ij} \quad \frac{1}{\rho}\overline{u_j\frac{\partial p}{\partial x_i}} \quad \overline{u_i\frac{\partial p}{\partial x_j}} \quad \underbrace{\frac{1}{\rho}\frac{\partial}{\partial x_j}\overline{p\,u_i} \quad \frac{1}{\rho}\frac{\partial}{\partial x_i}\overline{p\,u_j}}_{\text{pressure-transport}} \quad \underbrace{\overline{\frac{p}{\rho}\left(\frac{\partial u_i}{\partial x_j} \quad \frac{\partial u_j}{\partial x_i}\right)}}_{\text{pressure-strain}} \tag{47}$$

In wall-bounded flows, the pressure-transport contribution is usually small and we may seek closure for the pressure-strain part by considering the equation for the anisotropy in the "apparent" stresses in a statistically homogeneous field:

$$\frac{\partial a_{ij}}{\partial t} \quad \frac{1}{q^2}P_{ij} \quad a_{ij} \quad \frac{1}{3}\delta_{ij}P_{ss} \quad \frac{\Pi_{ij}}{q^2} \quad \frac{2\varepsilon_h}{q^2}(a_{ij} \quad e_{ij}) \tag{48}$$

where $P_{ij} \quad \overline{u_i u_k}\partial U_j/\partial x_k \quad \overline{u_j u_k}\partial U_i/\partial x_k$. From this equation, we deduce the asymptotic behavior of Π_{ij} as $a_{ij}/t \quad 0$ and $e_{ij} \quad a_{ij}$, which corresponds to the cases when the "apparent" stresses approach the limiting states of the axisymmetric disturbances located at the two-component limit:

$$\begin{array}{ll} (\Pi_{ij})_{2C\ \mathrm{iso}} \quad a_{ij}P_{ss} \quad \frac{1}{3}P_{ss}\delta_{ij} \quad P_{ij} \\ (\Pi_{ij})_{1C} \quad a_{ij}P_{ss} \quad \frac{1}{3}P_{ss}\delta_{ij} \quad P_{ij} \end{array} \tag{49}$$

Following the procedure suggested by Chou [13], the pressure-strain correlations can be evaluated exactly for statistically isotropic disturbances by parameterizing the volume integrals over two-point correlations and by utilizing only kinematic constraints. Tedious derivations, which were elaborated by Jovanovi} [19 (pp. 87-89)], yield:

$$\Pi_{ij} \quad \frac{3}{5}\ \frac{1}{3}P_{ss}\delta_{ij} \quad P_{ij}\ ,\ \ \mathrm{II}_a \quad 0 \tag{50}$$

The analytic behavior of $_{ij}$ given by (49) and (50) suggests an approximation for Π_{ij} in the following form:

$$\Pi_{ij} \quad a_{ij}P_{ss} \quad \mathcal{F}\ \frac{1}{3}P_{ss}\delta_{ij} \quad P_{ij} \tag{51}$$

where

$$\mathcal{F} \begin{array}{l} 0.6 \quad 3.6\,\frac{1}{2}\mathrm{II}_a \quad \frac{3}{4}\sqrt{\frac{2}{3}\mathrm{II}_a}^{\,3}\ ,\ \mathrm{III}_a \quad 0 \\ \\ 0.6 \quad 3.6\,\frac{1}{2}\mathrm{II}_a \quad \frac{3}{4}\sqrt{\frac{2}{3}\mathrm{II}_a}^{\,3}\ ,\ \mathrm{III}_a \quad 0 \end{array} \tag{52}$$

Determination of the transition criterion

Using the suggested forms for ε_{ij} and Π_{ij} given by (46) and (51) and also those for production and decay terms of the dissipation rate equation given by eqs. (19) and (20), the transport equations for the evolution of the statistically axisymmetric disturbances can be written as:

$$\frac{\partial \overline{u_i u_j}}{\partial t} \quad U_k \frac{\partial \overline{u_i u_j}}{\partial x_k}$$

$$P_{ij} \quad a_{ij}P_{ss} \quad \mathcal{F}\ \frac{1}{3}P_{ss}\delta_{ij} \quad P_{ij} \quad 2\mathcal{A}\varepsilon_h a_{ij} \quad \frac{2}{3}\varepsilon_h\delta_{ij} \quad \frac{1}{2}\nu\frac{\partial^2 \overline{u_i u_j}}{\partial x_k\,\partial x_k} \tag{53}$$

$$\frac{\partial \varepsilon_h}{\partial t} \quad U_k \frac{\partial \varepsilon_h}{\partial x_k} \quad 2\mathcal{A}\frac{\varepsilon_h \overline{u_i u_k}}{k}\frac{\partial U_i}{\partial x_k} \quad \psi\frac{\varepsilon_h^2}{k} \quad \frac{1}{2}\nu\frac{\partial^2 \varepsilon_h}{\partial x_k\,\partial x_k} \tag{54}$$

If we consider transition of the flow in a flat plate boundary layer with the aim of extracting a quantitative description of the interaction mechanism between the free stream disturbances and the boundary layer in the way proposed by Taylor [1], then the energy equation for the disturbances:

$$\frac{\partial k}{\partial t} \quad U_k \frac{\partial k}{\partial x_k} \quad P_k \quad \varepsilon_h \quad \frac{1}{2}\nu \frac{\partial^2 k}{\partial x_k \partial x_k} \tag{55}$$

which is obtained by contraction of eq. (53), immediately suggests stability towards small disturbances if the production is balanced by the dissipation:

$$P_k \quad \varepsilon_h \tag{56}$$

where $P_k = P_{ss}/2$.

The equilibrium constraint (56) reduces the energy equation to:

$$\frac{\partial k}{\partial t} \quad U_k \frac{\partial k}{\partial x_k} \quad \frac{1}{2}\nu \frac{\partial^2 k}{\partial x_k \partial x_k} \tag{57}$$

which is of boundary layer character and does not allow any amplification of statistically stationary disturbances in the boundary layer [25 (pp. 278-284)]. We conclude from eq. (57) that the energy k cannot grow in the boundary layer above the corresponding value of the free stream k_∞ and that the thickness of the fluctuating layer is larger than the boundary layer thickness.

Inserting (56) into the dissipation rate eq. (54):

$$\frac{\partial \varepsilon_h}{\partial t} \quad U_k \frac{\partial \varepsilon_h}{\partial x_k} \quad \underbrace{(2\mathcal{A} \quad \psi)}_{\substack{0 \\ \text{to insure} \\ \text{that } \varepsilon_h \quad 0}} \quad \frac{\varepsilon_h^2}{k} \quad \frac{1}{2}\nu \frac{\partial^2 \varepsilon_h}{\partial x_k \partial x_k} \tag{58}$$

and specifying that the dissipation rate is always positive, $\varepsilon \quad 0$, and at the critical point follows the energy k (as emerges from the work of Kolmogorov [23]), we deduce the transition criterion for small, statistically stationary and neutrally stable axisymmetric disturbances:

$$2\mathcal{A} - \psi \quad 0 \tag{59}$$

in terms of the Reynolds number Re_λ and the anisotropy II_a in the disturbances.

Hence, the derived transition criterion suggests the permissible magnitudes for the intensity q, the length scale λ, and the anisotropy II_a of disturbances that guarantee (56) ($P_k \quad \varepsilon_h$ with $\varepsilon_h \quad 0$) and therefore maintenance of the laminar flow regime in the flat plate boundary layer. The conservative criterion (59) restricts the magnitudes of Re_λ and II_a and prevents negative values of ε_h from developing locally within the boundary layer.

Analysis of the transition process in wall-bounded flows

The derived transition criterion (59) permits deductions to be made on the transition Reynolds number $(\mathrm{Re}_\lambda)_\mathrm{T}$ in terms of the anisotropy II_a in the disturbances. It should be remembered that the criterion must be satisfied across the entire shear layer starting

from the wall up to the outer edge of the boundary layer where the disturbances must match those of the free stream.

For axisymmetric disturbances, the wall is located in the anisotropy map either at the two component isotropic limit or at the one-component limit, which correspond to the configurations of the stresses with $III_a > 0$ and $III_a < 0$, respectively. Assuming that the axisymmetry axis of the disturbances is aligned along the mean flow direction, say x_1 so that $\lambda_i = (1, 0, 0)$, the analysis of the instantaneous fluctuations about the wall:

$$\begin{array}{llll} u_1 & a_1 x_2 & a_2 x_2^2 & \ldots \\ u_2 & & b_2 x_2^2 & \ldots \quad \text{as } x_2 \quad 0 \\ u_3 & c_1 x_2 & c_2 x_2^2 & \ldots \end{array} \tag{60}$$

involving the continuity equation leads to the conclusion that under common circumstances the disturbances at the wall must approach the one-component limit and that the two-component isotropic limit can be reached at the wall only under very special circumstances that can be considered more as an exception than the rule.

The question of transition and breakdown to turbulence induced by small axisymmetric disturbances which lie at the right-hand boundary of the anisotropy map and correspond to $III_a > 0$ was partially answered in the study by Jovanovi} and Hillerbrand [26]. Their analysis, based on kinematic considerations, shows that all coefficients of the Taylor series expansion (60) must vanish when the disturbances tend towards the one-component state: the disturbances at this state must satisfy the two-component limit and at the same time axisymmetry at large and small scales. The cross-plot of the dissipation rate at the wall *vs*. the anisotropy of turbulence at the wall shown in fig. 2 demonstrates in part that the above-mentioned analytical deduction is in agreement with the extrapolated trend from all numerical simulations of wall-bounded flows available. From the considerations outlined, we may conclude that

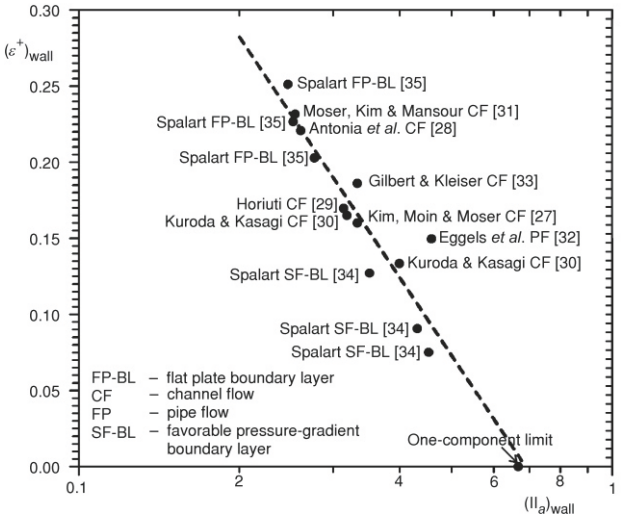

Figure 2. Turbulent dissipation rate at the wall, $\varepsilon \quad \nu(a_1^2 \quad c_1^2)$, normalized with the wall shear velocity and the kinematic viscosity of the flow medium *vs.* the anisotropy of turbulence III_a at the wall. A best-fit line through the numerical data extrapolates fairly well the expected trend as the one-component limit ($II_a = 2/3$) is approached

the near-wall region is absolutely stable to any level of the disturbances if $(II_a)_{wall} = 2/3$ and that this is a necessary but not sufficient condition that must be fulfilled for the persistence of a laminar regime in a flat plate boundary layer at infinite Reynolds numbers.

Analysis of the transition criterion which can be transformed for $III_a > 0$ as follows:

$$\frac{3}{2} \quad \frac{5}{6}\frac{1}{1 \quad 9\frac{1}{2}II_a \quad \frac{3}{4}\sqrt{\frac{2}{3}II_a}^{\,3}} \quad \mathcal{W} \quad 0 \tag{61}$$

forms the basis for the determination of the transition Reynolds number $(Re_\lambda)_T$ in terms of the anisotropy in the free stream disturbances. The distribution of $(Re_\lambda)_T$ as a function of II_a obtained from (61) is displayed in fig. 3 and suggests that transition and breakdown to turbulence can be avoided completely if the anisotropy in the free stream disturbances is sufficiently large:

$$(II_a)_\infty \quad 0.141 \tag{62}$$

The trajectory in the invariant map, which corresponds to absolutely stable disturbances, *i. e.* those disturbances for which the laminar regime in a flat plate boundary layer will persist up to very high Reynolds number, is shown in fig. 4. This figure also includes the results of direct numerical simulations of wall-bounded flows at different Reynolds numbers. The trends in the numerical results at the wall and at the channel centerline as Re Re_{crit} indicate that these tend towards the analytical result very closely and provide support for the theoretical considerations.

For $III_a > 0$ and vanishing anisotropy in the free stream disturbances, we infer from the results shown in fig. 3 that the transitional Reynolds number is given by:

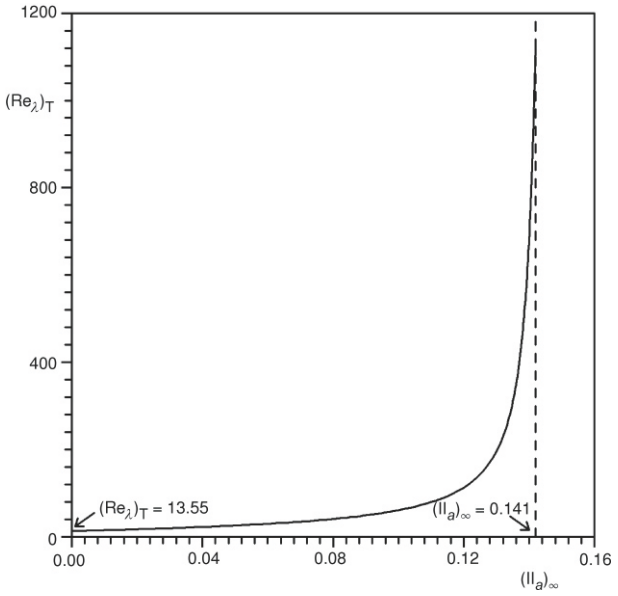

Figure 3. The transition Reynolds number $(Re_\lambda)_T$ as a function of the anisotropy II_a in the free stream disturbances

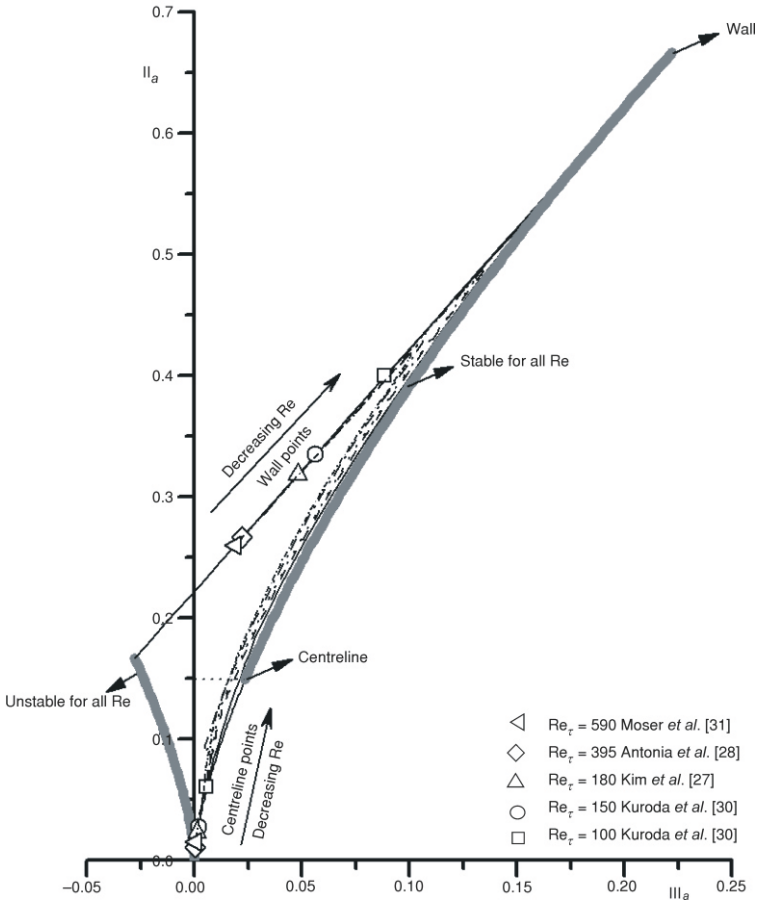

Figure 4. Anisotropy-invariant mapping of turbulence in a channel flow. Data, which correspond to low Reynolds number, show the trend as Re Re_{crit} towards the theoretical solution valid for small, neutrally stable, statistically stationary axisymmetric disturbances. The shading on the right-hand boundary of the map indicates the area occupied by the stable disturbances: for such disturbances it is expected that the laminar regime in a flat plate boundary layer will persist up to very high Reynolds numbers. The shading on the left-hand boundary of the map indicates the area occupied by the unstable disturbances: for such disturbances it is expected that turbulence will appear in the boundary layer at very low Reynolds numbers

$$(\mathrm{Re}_\lambda)_\mathrm{T} = 13.55 \quad \text{as} \quad (\mathrm{II}_a)_\infty \quad 0 \tag{63}$$

In order to translate $(\mathrm{Re}_\lambda)_\mathrm{T}$ into $(\mathrm{Re}_x)_\mathrm{T}$, the relation between the Taylor micro-scale λ and the boundary layer thickness δ is required. Using the exact expression

λ $(10)^{1/2} x_2$, which holds, however, only very close to the wall [16], the average value of $\overline{\lambda}$ across the boundary layer can be related to δ as follows:

$$\overline{\lambda} \quad \frac{\sqrt{10}}{2}\delta \tag{64}$$

Figure 5 shows that the above result together with relation (63) predicts variation of the transition Reynolds number with relative intensity of the free stream disturbances in fair agreement with the experimental data obtained under well-controlled laboratory conditions by Spangler and Wells [5]. Detailed discussion of the relation between theoretical deductions and other experimental results shown in fig. 5 is provided in section Concluding remarks.

We have already indicated that the axisymmetric disturbances corresponding to the configuration of the "apparent" stresses with $III_a < 0$, which require $\overline{u_1^2}$ $\overline{u_2^2}$ $\overline{u_3^2}$ are unlikely to appear in a flat plate boundary layer since such a form of the disturbances cannot satisfy the continuity equation in the region very close to the (smooth) wall. However, if the disturbances are forced to produce the above-mentioned form of the anisotropy, the transition criterion (59) suggests that for $III_a < 0$ it cannot be satisfied for any value of Re_λ

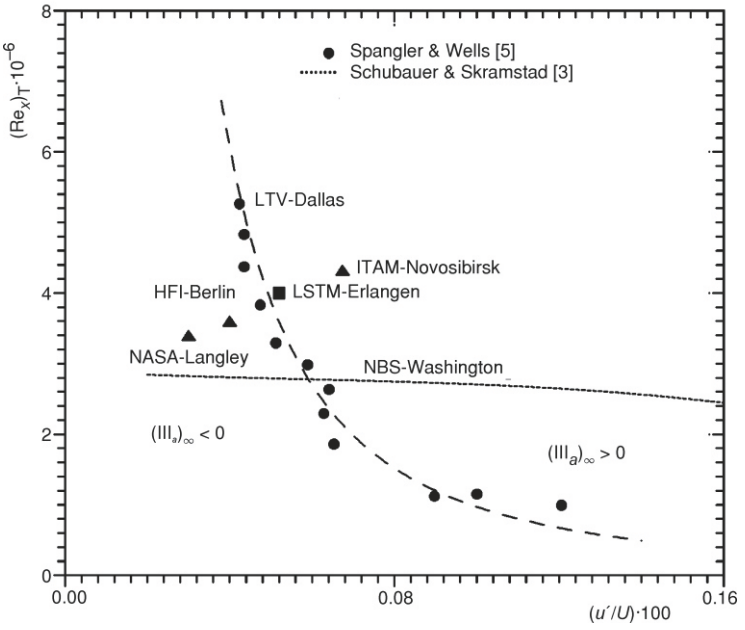

Figure 5. Comparison of the experimental data with prediction of the effect of free-stream disturbances on boundary layer transition; , Spangler and Wells [5]; , Schubauer and Skramstad [3]; , prediction of transition and breakdown to turbulence for vanishing anisotropy in the disturbances (II_a III_a 0, Re_{crit} = 13.55) with $\overline{\lambda}$ $10^{1/2} / 2\delta$ and δ $5(\nu x_1 / U_\infty)^{1/2}$

and we may therefore expect that under such circumstances turbulence will appear in the boundary layer at very low Reynolds numbers.

In a recent study, Lammers, Jovanovi}, and Durst [36] employed direct numerical simulations and succeeded in producing the anisotropy in the fluctuations corresponding to $III_a < 0$ and $\overline{u_1^2}$ $\overline{u_2^2}$ $\overline{u_3^2}$ very close to the wall by placing in a plane channel regularly spaced two-dimensional elements mounted at the wall and perpendicular to the flow direction. Using the lattice-Boltzmann numerical algorithm, they showed the existence of turbulence at a very low Reynolds number of Re 940 based on the centerline velocity and full channel height. Turbulence persisted over the entire computation time, which was sufficiently long to prove its self-maintenance. By examination of the statistical features of the flow across the anisotropy-invariant map, they found that these coincide with expectations emerging from the analysis of transition and breakdown to turbulence in a laminar boundary layer exposed to small, statistically stationary axisymmetric disturbances with the streamwise intensity component lower than the intensities in the normal and spanwise directions. Numerical experiments, carried out for different heights and streamwise spacing between roughness elements, revealed that it was possible to maintain turbulence at very low Reynolds numbers only if it reached the region close to the left-hand boundary of the anisotropy-invariant map.

Experimental investigations

The preceding theoretical considerations of transition and breakdown to turbulence led to the conclusion that, if the initially laminar boundary layer is exposed to low-intensity free stream turbulence of sufficiently high anisotropy, $(II_a)_\infty$ 0.14 and $(III_a)_\infty > 0$, the laminar regime in the boundary layer can be maintained up to very high Reynolds numbers.

In order to provide experimental support for the theoretical considerations, which are based on statistical techniques, a series of experiments were carried out in a wind tunnel in which the anisotropy in the free stream disturbances was only slightly lower than the corresponding criterion which guarantees stability of the boundary layer flow. However, the level of anisotropy in the free stream could only be quantified for low wind speeds and not for the high-speed range for which transition and breakdown to turbulence actually occurred in the boundary layer. In spite of this shortcoming, however, the experimental results presented here can be considered as exploratory and reflect in many significant details the trends inferred from the theoretical analysis.

Wind tunnel facility

The experiments were conducted in the return-type wind tunnel at the LSTM in Erlangen. Side and top views of the tunnel are shown in fig. 6. The flows driven by two fans with 12 blades each with the roots at a diameter of 1.12 m and the tips at a diameter of 2.0 m, yielding a maximum rpm value of 600. The fan was vibrationally isolated from the

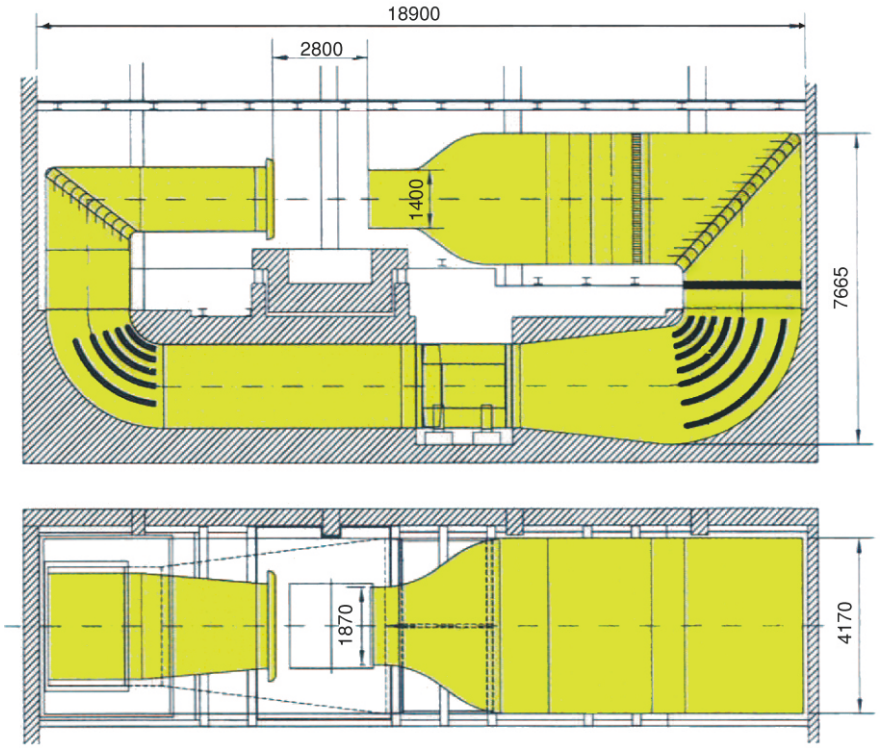

Figure 6. Side and top views of the return-type wind tunnel at the LSTM

rest of the tunnel. The 400 kW tunnel can be operated at a maximum speed of almost 65 m/s in the empty test section. Up to velocities of about 10 m/s there were no noticeable vibrations on the wind tunnel walls or the traversing system. If the velocity was increased above 10 m/s however, a vibration of the entire tunnel could be detected.

All diffusers in the wind tunnel circuit are designed to prevent flow separation. In the first diffuser upstream of the fan, a change from circular to rectangular cross-section is realized. A heat exchanger is situated downstream of the second diffuser after the fan. It has a capacity that allows a constant temperature (0.1%) to be maintained at all operating speeds. To eliminate flow disturbances from entering the test section, the settling chamber was equipped with a honeycomb to suppress swirl components while other flow disturbances were damped with a series of screens. The honeycomb has a depth of 200 mm and is composed of irregular hexagons with a wall thickness of 0.4 mm and an inner width of 25 mm. The mesh size of the screens is 0.71 mm (wire diameter 0.22 mm), yielding a blockage ratio of 57.08%. The distance between the three consecutive screens that are located on the downstream side of the honeycomb is 550 mm, which corresponds to more than 750 times the mesh size.

The shape of the contraction was determined from criteria of good flow uniformity and minimum risk of boundary layer separation near the inner corners. The smooth contraction of area ratio 5:1 is followed by a slight expansion. The contraction shape for height and width of the tunnel that reduces the cross-section from 3.13 × 4.17 to 1.40 ×1.86 m^2 is shown in fig. 7. The 2.0 m long test section is 1.86 m wide and 1.4 m high at the entrance. For experimental investigations with different measuring techniques there is a 3-D traversing system available that covers the entire test section. Additionally, a turntable is installed in the floor of the test section. The open test section provides a free stream mean velocity that remains constant within 0.2% with a free stream turbulence intensity of <0.3%. In order to provide satisfactory conditions for transition measurement, the test section was closed provisionally yielding a low turbulence intensity and a mean velocity angularity of 0.2°.

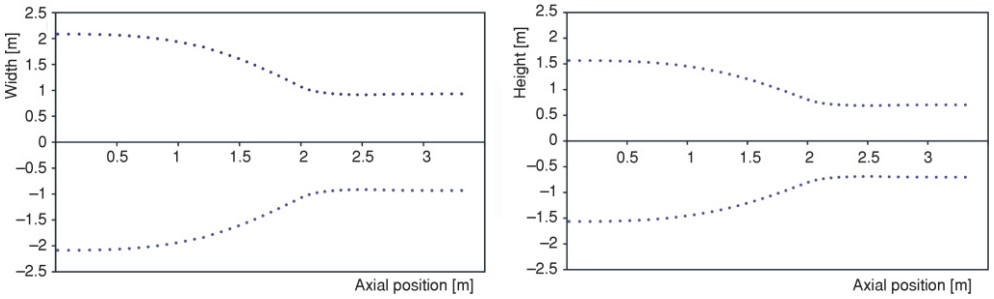

Figure 7. Shape of the contraction nozzle. The rectangular cross-section is reduced from 3.13 × 4.17 to 1.40 × 1.86 m^2 over a distance of 3.3 m, where the form of the contraction is different for height and width of the channel

Flat plate

The flat plate employed for transition measurements had the dimensions 1.2 × × 1.4 m^2 and a thickness of 10 mm. The plate, shown in fig. 8, was mounted vertically on the floor of the measuring section and extended over the height of the entire measuring section (fig. 9). The leading edge was designed to follow the NACA 0009 profile while the trailing edge reduces under an angle of 8° to a final thickness of 1 mm. The plate had a polished surface with surface roughness below 0.64 μm. The plate was originally used to test different measurement techniques in a laminar boundary layer disturbed with a purposely induced disturbance. For this reason there was a removable inlay of 0.2 × 0.7 m^2 in the center of the plate. Adjusting this inlay to the smallest possible step size results in remaining step heights between 30 and 50 μm. The dimensionless size of these steps decreases with increasing distance from the leading edge, yielding a maximum value of $\delta^+ = 2.7$, when normalized with wall friction velocity u_τ and the fluid viscosity ν, at a free stream speed of 60 m/s.

Two rows of holes can be found on the upper half of the plate. These were originally used to fix an LDA probe. These holes were covered with tape that had a thickness of 60 μm. Two strips of tape were placed along the plate in the flow direction starting at 130 and 140 mm after the leading edge and extending until the end of the trailing edge. At a free stream speed of 60 m/s the tape thickness corresponds to a maximum dimensionless thickness of $\delta^+ = 5.1$ at a distance of $x = 130$ mm from the leading edge. Owing to these disturbances on the plate, it was decided to take the measurements not in the center of the plate but at a distance of 0.4 m from the lower edge where the least influence of the surface roughnesses was detectable (see fig. 8).

Pressure distribution

Along the plate there are two rows of pressure taps installed that allow the determination of the local pressure gradient as shown in fig. 8. By mounting the plate on a turntable, which is located in the floor of the measuring section, the angle of attack can be adjusted. The criteria for best adjustment of the plate were determined by the largest possible constant pressure area in the flow direction. For the present investigation the pressure taps along the centerline of the plate were employed. Figure 10 shows the measured pressure gradient along the plate. After a distance of 200 mm from the leading edge, the deviation from a zero pressure gradient is below 0.5%.

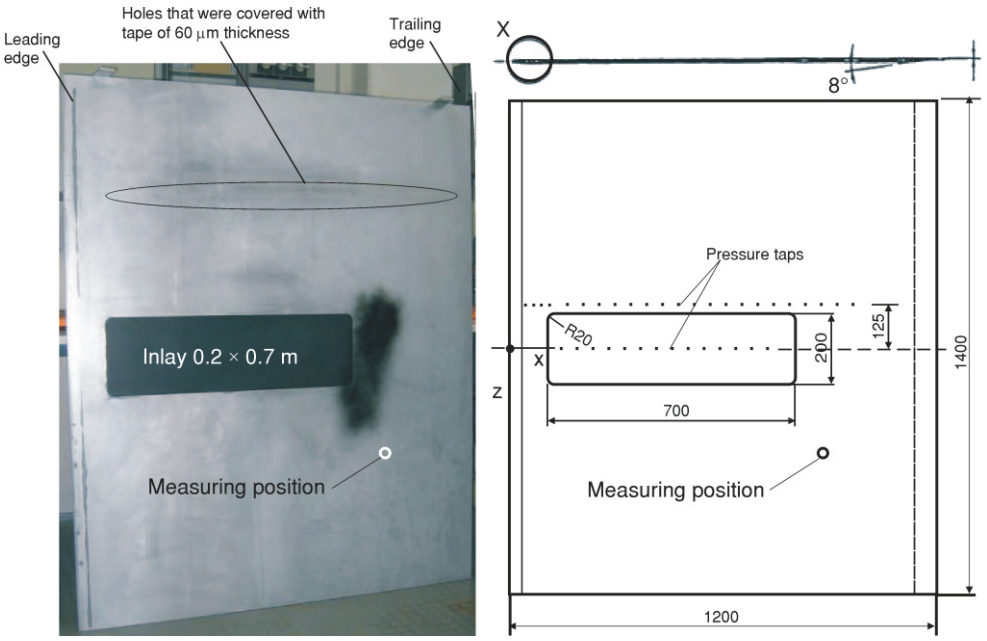

Figure 8. Flat plate used for transition investigation

To determine the influence of the pressure gradient on the development of the boundary layer, the dimensionless Λ parameter (that can be interpreted physically as the ratio of pressure forces to viscous forces) was calculated. It is given by:

$$\Lambda \quad \frac{\delta^2}{\nu}\frac{\mathrm{d}U_\infty}{\mathrm{d}x_1} \tag{65}$$

where δ is the boundary layer thickness according to the Blasius solution of the boundary layer equations. The velocity gradient $\mathrm{d}U_\infty/\mathrm{d}x_1$ can be expressed in terms of the measured pressure gradient $\mathrm{d}P/\mathrm{d}x_1$:

$$\frac{\mathrm{d}U_\infty}{\mathrm{d}x_1} \quad \frac{1}{\rho U_\infty}\frac{\mathrm{d}P}{\mathrm{d}x_1} \tag{66}$$

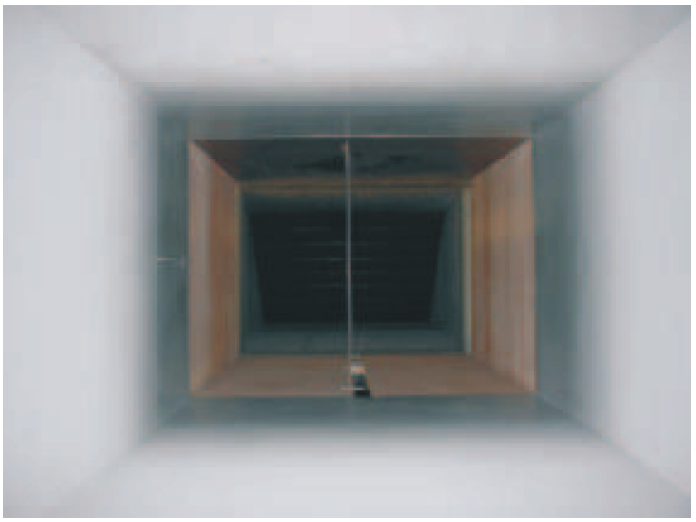

Figure 9. Flat plate vertically aligned in the closed test section of the LSTM wind tunnel

The value of the Λ parameter can serve as an indicator of the influence of the pressure gradient on the transition Reynolds number. For an adverse pressure gradient ($\Lambda < 0$), the transition Reynolds number is decreased whereas for favorable pressure gradients it is increased. The dependence of the Reynolds number associated with instability in the boundary layer on the Λ factor can be found in Schlichting [25 (p. 471)]. For $\Lambda = 0$, the Reynolds number which corresponds to instability based on the free stream velocity U_∞ and the displacement thickness δ_1, $\mathrm{Re}_{\delta_1} \quad U_\infty\delta_1/\nu$ is given by $(\mathrm{Re}_{\delta_1})_i = 645$. For $\Lambda = 1$ it increases to $(\mathrm{Re}_{\delta_1})_i = 800$ and for $\Lambda = -1$ it decreases to $(\mathrm{Re}_{\delta_1})_i = 400$.

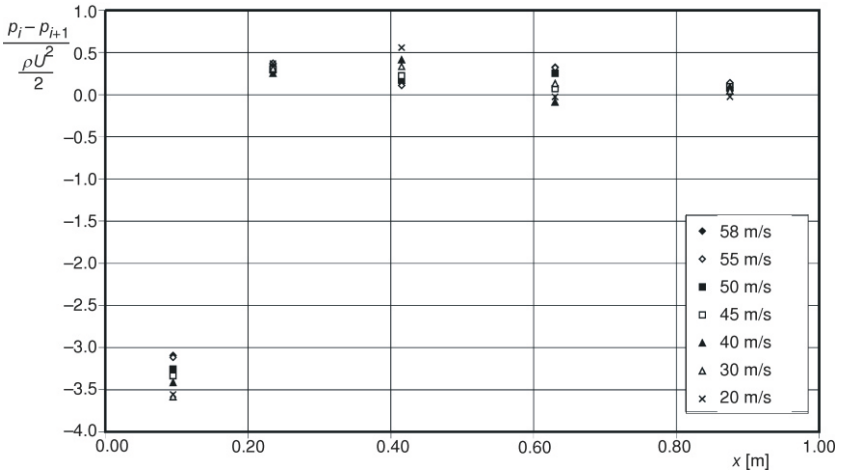

Figure 10. Deviation from zero pressure gradient along the flat plate

Figure 11 shows the Λ values obtained in the present experiment. It can be seen that they are significantly below $\Lambda = 0.2$ after a 200 mm distance from the leading edge. According to the linear theory of hydrodynamic stability [25], the resulting influence of the existing deviation from zero pressure gradient on $(\mathrm{Re}_{\delta_1})_i$ is therefore of the order of maximum 3%.

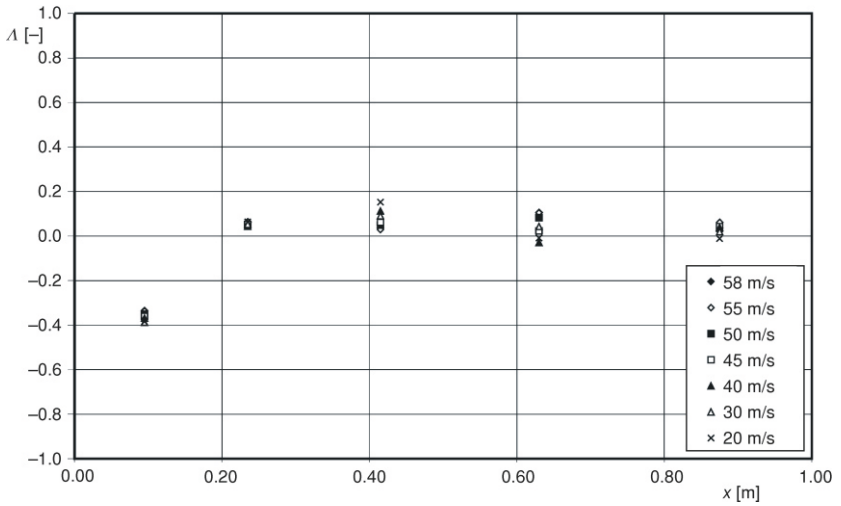

Figure 11. Value Λ as a function of downstream distance from the leading edge of the plate

Free stream intensity

Since the effect of free stream turbulence was expected to play an important role in the present investigation, special emphasis was placed on its measurements in order to examine the influence of anisotropy in the free stream disturbances on the boundary layer transition. The intensity of turbulence in the free stream was measured using three different hot-wire systems: DANTEC 55M, DANTEC 56C, and DANTEC Stream Line. Owing to its high signal-to-noise ratio, most of the measurements were performed with a DANTEC 55M system operated with a 55M10, standard bridge which provides reliable turbulence intensity measurements down to 0.015% of the freee stream at 10 kHz bandwidth and 10 m/s [37]. In order to minimize electronic noise from the hot-wire readings, the anemometers were carefully adjusted for optimum response by choosing appropriate settings for gain and bandwidth of the servo amplifier. Additionally, the output from the anemometers was low-pass filtered at 15 kHz, which was significantly higher than the energy-containing range of the free stream disturbances.

All measurements were conducted using a standard DANTEC 55P61 X-hot-wire probe operated at an overheat ratio of 0.8. In order to verify the low-intensity turbulence measurements obtained with the X-hot-wire probe, some control measurements of the streamwise intensity component were performed using a parallel DANTEC 55P71 hot-wire probe and employing the cross-correlation technique. The output signals from the anemometers were passed through back-up amplifiers, low-pass filtered and finally digitized using a 16-bit A/D converter.

The hot-wires were calibrated *in situ* in the wind tunnel by fitting the anemometer output voltage E to the effective cooling law $E^2 = A + BU_{\text{eff}}^{0.45}$. The coeffcients A and B were determined from the linear regression of the calibration data. Owing to small turbulence levels encountered in the free stream, the cosine law for the effective colling velocity U_{eff} was used for splitting the signals from the X-hot-wire into the velocity components. For yaw calibration, the method proposed by Bradshaw [38] was employed.

By orienting the probe holder in such a way that the hot-wires were lying in the x_1-x_2 plane, measurements of the streamwise u_1 and the normal u_2 components of the velocity fluctuations were performed. Rotation of the probe holder by 90º placed the hot-wires in the x_1-x_3 plane so that the streamwise and spanwise u_3 components of the velocity fluctuations could be measured.

At low free stream velocities (U_∞ 6-7 m/s), no noticeable vibrations of the test section walls and the traversing system were detected. For this wind speed range the free stream turbulence level in the empty test section was approximately $(\overline{u_1^2})^{1/2}/U_\infty$ 0.07% in the streamwise direction and $(\overline{u_2^2})^{1/2}/U_\infty$ $(\overline{u_3^2})^{1/2}/U_\infty$ 0.04% in the normal and lateral directions. Since turbulence of the free stream was almost axisymmetric, the above values of the intensity components yield the following estimate for the anisotropy of turbulence in the free stream:

$$(\text{II}_a)_\infty \quad 0.11 \tag{67}$$

$$(\text{III}_a)_\infty \quad 0.015 \tag{68}$$

For the above-mentioned wind speed range of the tunnel, Ye [39] and Schenck [40] measured, apart from the turbulence intensity components, also the turbulent dissipation rate of the free stream. From their measurements, which were obtained using specially designed arrays of X-hot-wire probes, one may obtain the value of the turbulent Reynolds number $(\mathrm{Re}_\lambda)_\infty$ as:

$$(\mathrm{Re}_\lambda)_\infty \quad 0.29 \tag{69}$$

Theoretical considerations of the transition process in wall-bonnded flows and the measured data of the anisotropy of turbulence in the free stream suggest that if the anisotropy is preserved at higher free stream velocities it would be possible to maintain a stable laminar regime in the boundary layer up to exceptionally high Reynolds numbers.

Transition detection and results

The arrangement of the wind tunnel test section with the model of a flat plate and associated instrumentation employed for investigations of laminar to turbulent transition were extensively tested by Fischer [41]. Using a standard DANTEC 55P15 boundary layer probe he verified that the flow development along the plate follows closely the Blasius solution of the boundary layer equations [25]. Results of Fischer's measurements obtained for the free stream velocity U_∞ 14 m/s are shown in fig. 12.

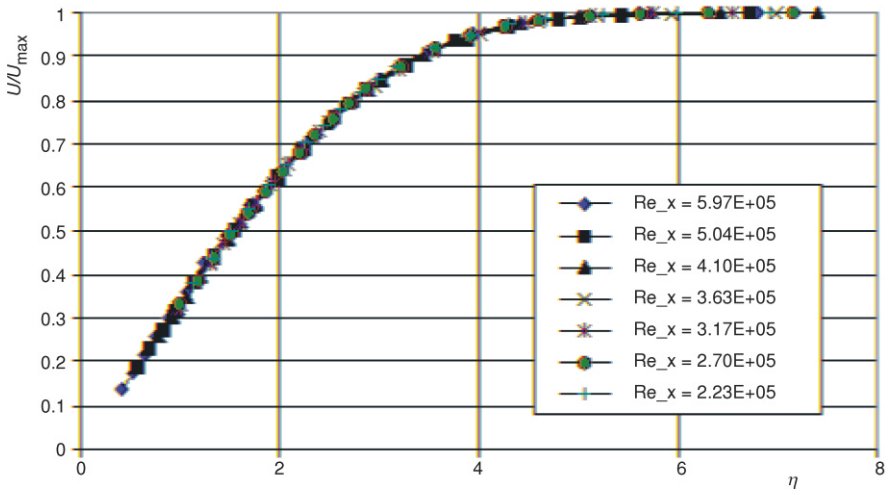

Figure 12. Velocity profiles measured in a laminar boundary layer over the flat plate, from Fischer [41]. Plotted is the normalized velosity U/U_∞ *vs.* normalized wall distance $\eta = x_2/(\nu x_1/U_\infty)^{1/2}$. The solid line corresponds to the Blasius solution of the boundary layer equations

For transition detection, a single DANTEC 55P11 hot-wire probe was glued on a razor blade of 0.4 mm thickness which was fixed to the flat surface with adhesive tape. No calibration was necessary since the level of fluctuations and not the actual velocity was of interest. For a laminar flow state there are only fluctuations arising from background turbulence observed in the signal and remain at a very low level. Intermittency and hence starting transition and breakdown to turbulence are detected by a jump in the fluctuation level.

For the first set of experiments, the surface-mounted hot-wire assembly was placed at a distance of 1 m from the leading edge. It was placed 1.3 mm from the surface and 0.4 m from the lower edge of the plate (see fig. 8). A central placement of the hot-wire on the plate was not chosen because of the surface roughness at this position caused by the tape that was used to cover existing holes in the plate. While the free stream velocity in the wind tunnel was gradually increased from rest up to 61.6 m/s (the maximum speed that could be obtained with the plate placed inside the test section), the hot-wire signals were recorded with a sampling frequency of 40 kHz and stored on a PC. At each intermediate velocity the hot-wire signals were recorded for 1 s after the velocity had been kept constant for about 15-20 minutes.

In a second set of experiments, the hot-wire assembly was moved along the plate with an increasing distance from the leading edge while the free stream velocity was kept constant at U_∞ 55 m/s. Thus the Reynolds number was increased by moving the hot-wire assembly further downstream. The signals were recorded at 0.3, 0.6, 0.9, 1.0, and 1.1 m distances from the leading edge. As in the first set of experiments, the hot-wire traces were recorded for 1 s at a sampling frequency of 40 kHz.

Since the entire test section started to vibrate at free stream velocities above U_∞ 10 m/s, additional measurements were performed by placing the hot-wire assembly on one of the side walls of the tunnel outside the test section. The hot-wire assembly was covered with a small box so that it was possible to distinguish between the influence of flow fluctuations and system vibrations. The hot-wire traces that were recorded outside the tunnel, and therefore at zero velocity, are shown in fig. 13. It is obvious from these traces that the apparent noise level which originates from system vibrations increases with increasing free stream velocity. The periodic signal that was recognized as typical for system vibrations had a frequency of about 300 Hz.

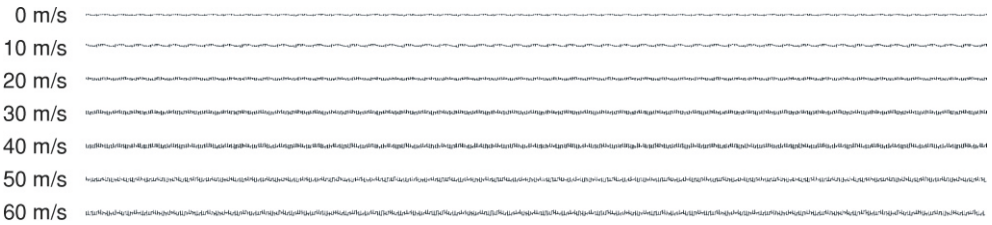

Figure 13. Hot-wire traces recorded outside the test section in order to determine the level of noise introduced by vibrations of the entire set-up

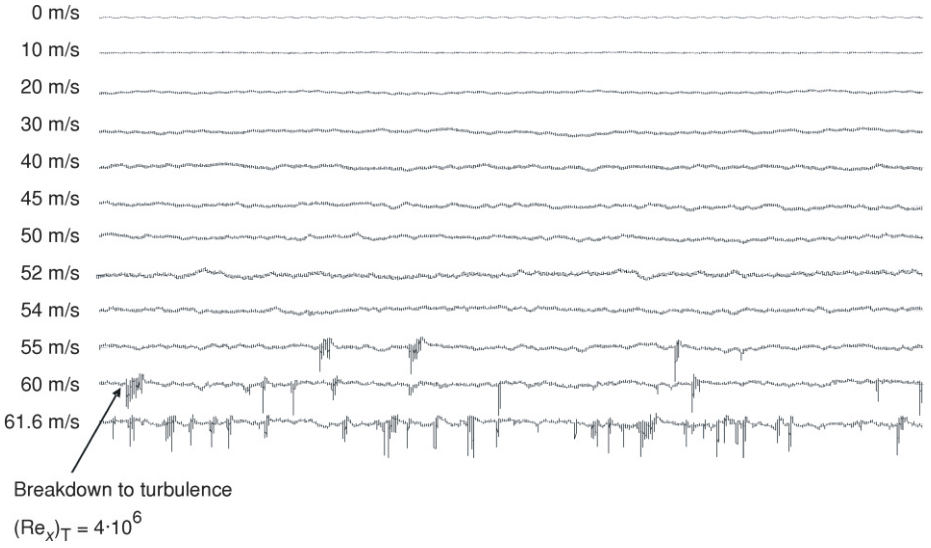

Figure 14. Hot-wire traces recorded at a distance of 1 m from the leading edge for increasing free stream velocities. The vertical and horizontal scales are the same as in fig. 13

The results from the first set of measurements with fixed downstream location of the hot-wire assembly and increasing free stream velocities can be seen in fig. 14. With increasing free stream velocity, the signal gradually became noisier so that the thickening of the baseline can be attributed to the system vibration as outlined above. On top of the signal carrying background turbulence and system vibrations, weak long-wave disturbances can also be seen but these show no tendency to organize in the way predicted by the linear theory of hydromechanic stability. At a free stream velocity of U_∞ 55 m/s the first signs of intermittency, characterized by the appearance of isolated spikes in the signal were observed. For this free stream velocity, the intermittency factor defined as:

$$\gamma \quad \lim_{T \infty} \frac{1}{T} \int_0^T I(t)\mathrm{d}t \tag{70}$$

where $I(t)$ is the intermittency function:

$$I(t) \quad \begin{matrix} 1, & \text{turbulent} \\ 0, & \text{laminar} \end{matrix} \tag{71}$$

was fairly low at γ 3.7%. Figure 14 shows that with further increase in the free stream velocity, the number of intermittently appearing spikes in the signal increases. At the maximum free stream velocity of U_∞ 61.1 m/s a turbulent state is reached at the measuring location on the plate. From the hot-wire traces shown in fig. 14, we may conclude that the Reynolds number which corresponds to transition and breakdown to

turbulence can be estimated based on a free stream velocity of U_∞ 60 m/s, yielding a value of $(Re_x)_T$ $4 \cdot 10^6$. The results from the second set of measurements in which the free stream velocity was kept constant and the hot-wire assembly was placed at various locations along the plate are shown in fig. 15. We may note, by inspection of the hot-wire traces, that the noise level due to the background turbulence and the system vibrations remains constant. At a distance of 1 m from the leading edge of the plate, first evidence of intermittency is observed with rather isolated spikes in the signal. The observed spikes appear only in a very small time fraction of the signal, corresponding to γ 3-4%. At a distance of 1.1 m from the leading edge, the number of spikes in the signal increased significantly, so that the transition Reynolds number based on this value can be estimated as the same value of $(Re_x)_T$ $4 \cdot 10^6$ that was obtained in the first set of experiments.

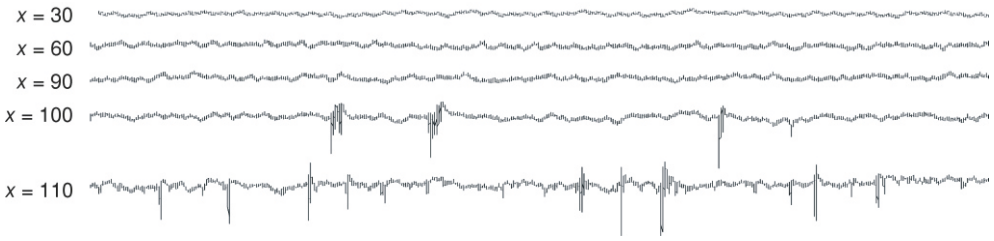

Figure 15. Hot-wire traces recorded at various distances from the leading edge for a fixed free stream velocity of U_∞ = 55 m/s

Concluding remarks

It is a generally accepted (dogmatic) view nowadays that much is known about early stages of transition and breakdown to turbulence from previous theoretical and experimental investigations which account for transition from stability considerations in which amplification or damping of infinitesimal disturbances is determined from the Orr-Sommerfeld equation in terms of the Reynolds number and the frequency or the wavelength of the disturbances. In this respect, early theoretical work of Tollmien [42] and Schlichting [43] together with the experimental study of Schubauer and Skramstad [3] form the starting point and a solid basis for providing understanding of the basic mechanism involved, so that little further investigation is required. Much of the current work follows this line of thinking about transition and the origin of turbulence in the boundary layer.

We do know, however, that the theory of small disturbances falls into difficulties when an attempt is made to provide an explanation for the nature of transitions in confined wall-bounded flows such as channel or pipe flows. For the latter case, the theory leads to the surprising result that the pipe flow is stable for infinitesimal disturbances at all Reynolds numbers. Schlichting [25] was quite right in pointing out that:

"We have to reconsider the relation between the theory of small disturbances as to whether transition can always be said to be due to an amplification of small disturbances".

Anisotropy-invariant mapping of boundary layer oscillations using results deduced from the theory of small disturbances shown in figs. 16 and 17 reveals that the mechanism responsible for instability and therefore for the initial phase of transition displays an anomalously complex trajectory across the anisotropy-invariant map which is inconsistent with the trend in the behavior of turbulence as the critical Reynolds number is approached (see fig. 4): the trajectory sweeps along the two-component state back and forth between the one-component limit and the isotropic two-component limit. Such a tendency in the invariant domain implies that solutions obtained from the theory of small disturbances can explain an exceptional scenario of transition rather than the rule and as such can be expected to be applicable in unusual circumstances only.

With respect to the analysis of the transition process in wal-bounded flows, we may note that the energy components of the disturbances, shown in fig. 16, do not exhibit the expected trend which matches the kinematic constrains valid for the one-component state of the disturbances: the slopes of both of the distributions shown in fig. 16 must decrease and vanish at the wall so that the dissipation rate also vanishes at the wall and thereby satisfies constraints valid at the one-component limit (see fig. 2).

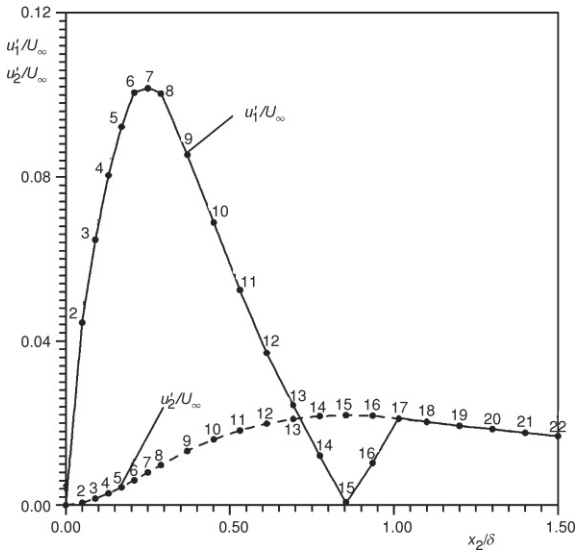

Figure 16. Distributions of component energies $u_1 \quad (\overline{u_1^2})^{1/2}$ and $u_2 \quad (\overline{u_2^2})^{1/2}$ normalized with the free stream velocity U_∞ of boundary layer oscillations according to Schlichting [42]. Points are labeled with numbers in order that the position can be identified on the trajectory across the anisotropy invariant map shown in fig. 17

An important issue associated with the nature of transition in the boundary layer is related to the role of sound disturbances, which accounted for approximately 90% of the total disturbance energy in the wind tunnel experiments of Schubauer and Skramstad [3]. By conducting a similar study in a specially designed test facility in which noise due to sound disturbances as well as mechanical vibrations could be completely eliminated, Spangler and Wells [5] were able to show that the effect of acoustic noise leads to misleading evaluation and interpretation of the experimental data. By examination of the energy spectra of the free stream disturbances, they concluded that the results reported by Schubauer and Skramstad [3] on natural

transition correspond to the stability of laminar boundary layer exposed to intense acoustic disturbances.

The above-discussed influence of the acoustic noise in the free stream disturbances may therefore explain in part completely different trends in the results shown in fig. 5, which display the effect of free stream turbulence on the transition Reynolds number from various published results. In contrast to the data obtained in the presence of an intense acoustic field, which show nearly a constant value of $(\mathrm{Re}_x)_\mathrm{T}$ for a low turbulence level, for the experimental data which correspond to flow conditions almost without any acoustic disturbances the transition Reynolds number displays a continuous increase with decreasing free stream turbulence level. Figure 5 demonstrates that the latter data are in close agreement with predictions obtained from the presented theoretical analysis of the transition process in the boundary layer.

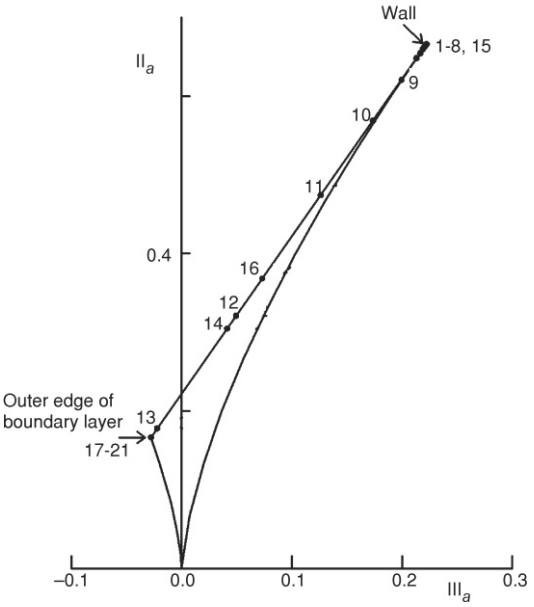

Figure 17. Anisotropy-invariant mapping of boundary layer oscillations on a flat plate using results obtained from the stability analysis towards small disturbances displayed in fig. 16

The results of transition measurements presented for $(\mathrm{Re}_x)_\mathrm{T}$ $4\cdot10^6$, which are included in fig. 5, agree very well with the data of Spangler and Wells [5] and lie close to the analytical prediction obtained for vanishing anisotropy of free stream disturbances. This suggests that the level of free stream turbulence remained unchanged and that the anisotropy decreased with increasing free stream velocity for the experiments described (section Experimental investigations).

The results presented in fig. 5 show that two sets of measurements which were obtained in the former NASA-Langley stability tunnel and at the Herman-Föttinger Institute in Berlin lie under the curve showing the predicted variation of $(\mathrm{Re}_x)_\mathrm{T}$ with the intensity of free stream turbulence and therefore display a lower value of $(\mathrm{Re}_x)_\mathrm{T}$ than expected for $(\mathrm{II}_a)_\infty = 0$. We do not know the true effective level of external turbulence $Tu = [(1/3)(\overline{u_1^2} \quad \overline{u_2^2} \quad \overline{u_3^2})]^{1/2}/U_\infty$ and the actual level of the anisotropy in the free stream for these experiments and can only suspect that owing to high contraction ratios of the wind tunnels mentioned, 9:1 and 18:1 respectively, the character of the anisotropy was $(\mathrm{III}_a)_\infty < 0$ for which the theoretical consideration in section Analysis of the transition process in wall-bounded flows, predict transition to occur earlier than for $(\mathrm{III}_a)_\infty > 0$.

Reasoning similar to that presented above may be applied for the interpretation of the transition data acquired in the ITAM wind tunnel in Novosibirsk, Russia. Figure 5

shows that these data lie above the analytic prediction and display a higher value of $(Re_x)_T$ than expected for $(II_a)_\infty = 0$. The theoretical considerations in the same section suggest that this might be due to the small favorable anisotropy $(III_a)_\infty > 0$ present in the free stream disturbances.

Acknowledgments

This research received financial support from the Deutsche Forschungsgemeinschaft (DFG) within the project Du 101/54-3. The authors gratefully acknowledge this support. We are grateful for stimulating discussions that we had with Dipl.-Ing. Herman Lienhart and Dr.-Ing. Stefan Becker during various phases of the experimental work reported here.

References

[1] Taylor, G. I., Statistical Theory of Turbulence. Part V. Effects of Turbulence on Boundary Layer. Theoretical Discussion of Relationship between Scale of Turbulence and Critical Resistance of Spheres, *Proc. Roy. Soc. Lond. A, 156* (1936), pp. 307-317
[2] Dryden, H. L., Air Flow in the Boundary Layer Near a Plate, NACA Report No. 562, USA, 1936
[3] Schubauer, G. B., Skramstad, H. K., Laminar-Boundary-Layer Oscillation and Transition on a Flat Plate, NACA Report No. 909, USA, 1943
[4] Wells, C. S., Effects of Free Stream Turbulence on Boundary-Layer Transition, *AIAA J., 5*, (1967), pp. 172-174
[5] Spangler, J. G., Wells, C. S., Effects of Free Stream Disturbances on Boundary-Layer Transition, AIAA J., *6* (1968), pp. 534-545
[6] Saric, W. S., Reynolds, G. A., Experiments on the Stability and Nonlinear Waves in a Boundary Layer, in: Laminar-Turbulent Transition (Eds. E. Eppler, H. Fasel), Springer-Verlag, Berlin, 1980, pp. 125-134
[7] Kachanov, Y. S., Kozlov, V. V., Levchenko, V. Y., The Origin of Turbulence in the Boundary Layer (in Russian), Nauka, Novosibirsk, USSR, 1982
[8] Pfenninger, W., Transition Experiments in the Inlet Length of Tubes at High Reynolds Numbers (Ed. G. V. Lachmann), in: Boundary Layer and Flow Control, Vol. 2, Pergamon Press, Oxford, UK, 1961, pp. 970-980
[9] Hinze, J. O., Turbulence, 2nd ed., McGraw-Hill, New York, USA, 1975
[10] Jovanović, J., Pashtrapanska, M., Frohnapfel, B., Durst, F., Koskinen, J., Koskinen, K., On the Mechanism Responsible for Turbulent Drag Reduction by Dilute Addition of High Polymers: Theory, Experiments Simulations and Predictions, *J. Fluids Eng., 128* (2006), pp. 118-130
[11] Jovanović, J., Pashtrapanska, M., On the Criterion for the Determination Transition onset and Breakdown to Turbulence in Wall-Bounded Flows, *J. Fluids Eng., 126* (2004), pp. 626-633
[12] Rotta, J. C., Turbulent Flows: An Introduction into Theory and Its Application (in German), Teubner, Stuttgart, Germany, 1972, pp. 120-127
[13] Chou, P. Y., On the Velocity Correlation and the Solution of the Equation of Turbulent Fluctuation, *Q. Appl. Math., 3* (1945), pp. 38-54
[14] Lumley, J. L., Newman, G., The Return to Isotropy of Homogeneous Turbulence, *J. Fluid Mech., 82* (1977), pp. 161-178

[15] Kolovandin, B. A., Vatutin, I. A., Statistical Transfer Theory in Non-Homogeneous Turbulence, *Int. J. Heat. Mass Transfer, 15* (1972), pp. 2371-2383
[16] Jovanović, J., Ye, Q.-Y., Durst, F., Statistical Interpretation of the Turbulent Dissipation Rate in Wall-Bounded Flows, *J. Fluid Mech., 293* (1995), pp. 321-347
[17] Jovanović, J., Ye, Q.-Y., Durst, F., Refinement of the Equation for the Determination of Turbulent Micro-Scale, Universität Erlangen-Nürnberg Rep., Germany, LSTM 349/T/92, 1992
[18] Jovanović, J., Otić, I., Bradshaw, P., On the Anisotropy of Axisymmetric Strained Turbulence in the Dissipation Range, *J. Fluids Eng., 125* (2003), pp. 410-413
[19] Jovanović, J., The Statistical Dynamics of Turbulence, Springer-Verlag, Berlin, 2004
[20] Lumley, J. L., Computational Modeling of Turbulent Flows, *Adv. Appl. Mech., 18* (1978), pp. 123-176
[21] Jovanović, J., Otić, I. On the Constitutive Relation for the Reynolds Stresses and the Prandtl-Kolmogorov Hypothesis of Effective Viscosity in Axisymmetric Strained Turbulence, *J. Fluids Eng., 122* (2000), pp. 48-50
[22] Rotta, J. C., Statistical Theory of Non-Homogeneous Turbulence (in German), *Z. Phys., 129* (1951), pp. 547-572
[23] Kolmogorov, A. N., On Degeneration of Isotropic Turbulence in an Incompressible Viscous Liquid (in Russian), Dokl. Akad. Nauk SSSR, *6* (1941), pp. 538-540
[24] Sreenivasan, K. R., On the Scaling of the Turbulence Energy Dissipation Rate, *Phys. Fluids, 27* (1984), pp. 1048-1051
[25] Schlichting, H., Boundary-Layer Theory, 6th ed., McGraw-Hill, New York, USA, 1968
[26] Jovanovi}, J., Hillerbrand, R., On Peculiar Property of the Velocity Fluctuations in Wall-Bounded Flows, *Thermal Science, 9* (2005), 1, pp. 3-12
[27] Kim, J., Moin, P., Moser, R., Turbulence Statistics in a Fully Developed Channel Flow at Low Reynolds Numbers, *J. Fluid Mech., 177* (1987), pp. 133-166
[28] Antonia, R. A., Teitel, M., Kim, J., Browne, L. W. B., Low-Reynolds Number Effects in a Fully Developed Channel Flow, *J. Fluid Mech., 236* (1992), pp. 579-605
[29] Horiuti, K., Miyake, Y., Miyauchi, T., Nagano, Y., Kasagi, N., Establishment of the DNS Database of Turbulent Transport Phenomena, Rep. Grants-in-aid for Scientific Research, No. 02302043, 1992
[30] Kuroda, A., Kasagi, N., Hirata, M., Direct Numerical Simulation of the Turbulent Plane Couette-Poiseulle Flows: Effect of Mean Shear on the Near Wall Turbulence Structures, *Proceedings*, 9th Symposium on Turbulent Shear Flows, Kyoto, Japan, 1993, 8.4.1-8.4.6
[31] Moser, R. D., Kim, J., Mansour, N. N., Direct Numerical Simulation of Turbulent Channel Flow up to Re_τ = 590, *Phys. Fluids, 11* (1999), pp. 943-945
[32] Eggels, J. G. M., Unger, F., Weiss, M. H., Westerweel, J., Adrian, R. J., Friedrich, R., Nieuwstadt, F. T. M., Fully Developed Turbulent Pipe Flow: A Comparison between Direct Numerical Simulation and Experiment, *J. Fluid Mech., 268* (1994), pp. 175-209
[33] Gilbert, N., Kleiser, L., Turbulence Model Testing with the Aid of Direct Numerical Simulation Results, *Proceedings*, 8th Symposium on Turbulent Shear Flows, Munich, Germany, 1991, 26.1.1-26.1.6
[34] Spalart, P. R., Numerical Study of Sink-Flow Boundary Layers, *J. Fluid Mech., 172* (1986), pp. 307-328
[35] Spalart, P. R., Direct Simulation of a Turbulent Boundary Layer up to R_Θ = 1410, *J. Fluid Mech., 187* (1988), pp. 61-98
[36] Lammers, P., Jovanović, J., Durst, F., Numerical Experiments on Wall-Turbulence, *Thermal Science, 10* (2006), pp. 33-62 (in this issue)
[37] ***, DANTEC Instruction Manual for DISA CTA, 1976
[38] Bradshaw, P., An Introduction to Turbulence and Its Measurements, Pergamon Press, Oxford, UK, 1971
[39] Q.-Y., Ye, The Turbulent Dissipation of Mechanical Energy in Shear Flows (in German), Ph. D. thesis, University Erlangen-Nurenberg, Germany, 1996

[40] Schenck, T. C., Measurements of the Turbulent Dissipation Rate in Plane and Axisymmetric Wake Flows, University Erlangen-Nurenberg, Ph. D. thesis, Germany, 1999
[41] Fischer, M., Turbulent Wall-Bounded Flows at Low Reynolds Numbers (in German), Ph. D., thesis, University Erlangen-Nurenberg, Germany, 1999
[42] Tollmien, W., On the Formation of Turbulence (in German), 1. Mitteilungen, Nachr. Ges. Wiss. Göttingen, Math. Phys. Klasse, pp. 21-44, 1929
[43] Schlichting, H., Amplitude Distribution and Energy of Small Disturbances in a Flat Plate Boundry Layer (in German), Nachr. Ges. Wiss. Göttingen, *Math. Phys. Klasse, Fachgruppe I, 1*, pp. 47-78, 1935

Authors' address:

J. Jovanović, B. Frohnapfel, E. Škaljić, M. Jovanović
Lehrstuhl für Strömungsmechanik
Universität Erlangen-Nürnberg
Cauerstrasse, 4, D-91058, Germany

Corresponding author (J. Jovanović):
E-mail: jovan@lstm.uni-erlangen.de.

Paper submitted: May 30, 2006
Paper revised: June 3, 2006
Paper accepted: June 15, 2006